Materials International
Open Access Journal (ISSN: 2668-5728)

Article
Volume 7, Issue 4, 2025, 33
https://doi.org/10.33263/Materials74.033

Green Synthesized ZnO/Polymer Nanocomposites Using Calotropis gigantea for Biomedical Applications and Docking Studies

Kalpana [1], G. Kavitha [1], G. Dinesh Kumar [1,*], S. Mohana Priya [2]

[1] Gobi Arts and Science College, Gobichettipalayam 638 453, Tamilnadu.; kkalpanachem@gmail.com (K.); gkavitha@gascgobi.ac.in (G.K.); dineshchem@gascgobi.ac.in (G.D.K.);
[2] Kumaragiriscihub, Salem 636002, Tamil Nadu, India; priyaechem@gmail.com;
* Correspondence: gkavitha@gascgobi.ac.in;

Received: 12.02.2025; Accepted: 1.08.2025; Published: 10.12.2025

Abstract: Nanosized organic and inorganic particles are progressively gaining popularity in medical applications. The ongoing research focuses on the synthesis of zinc oxide nanoparticles (ZnO NPs) applying microwave irradiation and an aqueous extract of *Calotropis gigantea* flowers as a bio-reducing agent. Furthermore, cellulose and polyvinyl alcohol polymer composites of ZnO nanoparticles were synthesized and characterized spectrally. Various techniques were employed to investigate the production, geometry, crystalline structure, elemental composition, and absorption band of the materials. The antibacterial activity of the substance was found to be the most effective compared to other samples studied. ZnO/polymer nanocomposites demonstrate potential cytotoxicity against the HT-29 human colon cancer cell line. MTT assays showed that the inhibitory concentration with IC_{50} values of 44.7 ± 0.05 µg/mL and 51.53± 0.05 µg/mL, respectively, for cellulose and polyvinyl alcohol derivatives.

Keywords: bio extract; polymer nanocomposite; antimicrobial assay; anticancer property.

1. Introduction

The versatility of biogenic nanocomposites, with their biological activities, biodegradability, nontoxicity, easy availability, and abundance, has sparked interest. Metal oxide/polymer nanocomposites have been thoroughly investigated [1,2]. The growing importance of nanomaterials across sectors such as biomedical, agricultural, energy, environmental health, and industrial has led to increased interest in environmentally friendly, green, or biological methods for synthesizing nanometallic particles [3,4]. ZnO has a substantial exciton binding energy of 60 meV and operates as an n-type semiconductor with a bandgap measuring around 3.37 eV, displaying excellent antimicrobial efficacy, low cytotoxicity, and spin dynamics [5,6]. The global ZnO market is witnessing a growth rate of 4.03% annually. ZnO is extensively applied in innumerable sectors due to its remarkable chemical, physical, and biological properties. Generally, the characteristics of ZnO, such as its band gap, crystallite size, and morphology, are dictated by the synthesis methods and parameters utilized. The desirable antimicrobial, anti-inflammatory, and anticancer properties

of ZnONP make it ideal for biomedical applications, including its use in sunscreens owing to its unique ultraviolet ray-scattering properties, drug-delivery mechanisms, and wound-healing applications. With an understanding of the potential applications of ZnO nanoparticles, our aim is to develop stable ZnO nanoparticles via microwave irradiation using aqueous Calotropis gigantea flowers as a bio-reducing agent, to evaluate the biological activities of ZnO and its polymer composites. The microbicidal properties of these nanoparticles are attributed to their stability in the growth medium, which allows for extended interaction with bacteria. Developing stable nanoparticles that can effectively inhibit pathogen activity is a key focus of research. The generation of nanoscale ZnO is largely governed by a combination of physical and chemical techniques [7, 8]. Physical methods include chemical vapor deposition, thermal evaporation, pulsed laser deposition, molecular beam epitaxy, and metal-organic chemical vapor deposition, among others. These procedures generally require high vacuum environments and consume significant energy. On the other hand, chemical methods such as sol-gel, solvothermal, sonochemical, hydrothermal, electrodeposition, and spray pyrolysis are more economical and conducive to large-scale production. Yet, they are detrimental to the environment [9]. Nevertheless, the high cost of reagents and equipment, coupled with the environmental risks associated with physical and chemical analysis, has presented obstacles in the synthesis of ZnO NPs.

It is essential to develop innovative biocompatible techniques to overcome these limitations in nanomaterial production. In this regard, the plant extract-mediated green synthetic approach is preferred due to its environmental friendliness, low cost, minimal contaminants, short duration, and high purity product [10]. The consistent updating of the natural extract synthesis is environmentally beneficial and safe. This approach facilitates the production of a wide variety of nanoscale materials, including metals, oxides, alloys, and sulfides. Research demonstrates the use of various plant extracts in the manufacturing of ZnO nanoparticles, encompassing leaves, fruits, seeds, roots, and entire plants. These biological matrices contain phytochemicals such as phenolic compounds, alkaloids, flavonoids, and terpenoids, which contribute to the bio-reduction mechanism and serve as stabilizing and reducing agents.

Recently, biosynthesized Chitosan/ZnO/polysaccharide composite was reported to show enhanced biological characteristics [11]. One-pot synthesis of antitumor chitosan/ZnO nanocomposite has also been studied [12]. The *in situ* green-synthesized nanocomposite of zinc oxide/hyaluronan biopolymer has been demonstrated to exhibit pronounced anti-tumor properties [13]. At the same time, the biomedical applications of ZnO/cellulose have been studied by Mazhar et al. [14]. Similarly, ZnO/PVA synthesis using *Moringa oleifera* leaf extract template and its biological evaluation has been investigated by Dejen *et al.* [15], as well as biosynthesis of ZnO nanoparticles derived from *Capparis zeylanica* leaf extract [16]. A carboxymethyl cellulose/Zinc oxide (ZnO) composite prepared by the solution-casting technique exhibits enhanced UV shielding properties, as demonstrated by Badry *et al.* [17]. The multifunctional potential of ZnO@CA/PCL nanocomposites, exhibiting promising in vitro anticancer activity, has also been investigated recently [18]. ZnO-g-PCLDLA core–shell nanoparticles with outstanding antimicrobial activity were studied recently [19].

The proposed research highlights the production of nano ZnO and its polymer composite treated with the Calotropis gigantea flower extract as a green reducing agent. *Calotropis gigantea*, also known as the crown flower or giant milkweed, is a plant native to Asia and has been traditionally used in medicine for various ailments [20]. Hence, the

application of nanoparticles_in electronics, medical, and food industries is intensifying. ZnO/polymer composites have attained a prominent status among crucial technological materials, owing to their diverse applications driven by unmatched electrical, thermal, mechanical, optical, catalytic, and biomedical properties. A key strategy for the synthesis of ZnO/polymer nanocomposites is based on specific structural arrangements, in which the distinct structural forms of conventional metal oxides, such as ZnO, in combination with polymers, achieve the desired performance metrics. To the best of our knowledge, only a few studies are available on the synthesis of cellulose and polyvinyl alcohol ZnO NPs; therefore, we aim to shed light on this topic by physically and chemically characterizing nano ZnO and its polymer composite, as well as exploring its potential antimicrobial applications.

2. Materials and Methods

2.1. Materials.

Zinc acetate and Sodium hydroxide are procured from SD Fine Chemicals. Cellulose [99% pure], Polyvinyl alcohol [with an average molecular weight of 125,000 and 98% purity] are acquired from Sigma Aldrich. All chemicals were used without further purification, and Calotropis gigantea was collected in the Shevarayan Hills region, Salem, India.

2.2. Preparation of aqueous Calotropis gigantea flower extract.

10 g of *Calotropis gigantea* blossoms were submerged in alcohol for an hour after being thoroughly cleaned with lots of distilled water and gently rubbed with it. The material was heated to 60°C for 30 min in 100 mL of distilled water. The extract was allowed to cool, and to achieve a uniform concentration, the mixture was agitated using centrifugation. For later usage, the finished filtrate was kept in a dry, cool place.

2.3. Microwave synthesis of ZnO NP and Polymer composites.

ZnO NPs were synthesized by mixing 6 g of zinc acetate and 25 mL of bio extract, which were mixed homogenously. The pH of the resulting mixture was kept above 10 by adding 1 M NaOH. The admixture was exposed to a microwave reactor and irradiated for 30s under 800W. The above technique was performed in the presence of 1wt.% of cellulose or polyvinyl alcohol to obtain polymeric composites. The resultant solution was filtered, dried, and used for further studies. The polymeric composite of ZnO/cellulose and ZnO/polyvinyl alcohol were termed as ZCE and ZPL, respectively, hereafter. All samples were calcined for 2 hours at 400°C. Different techniques were used to characterize the resulting materials.

2.4. Characterization of ZnO, ZCE, and ZPL.

The physical, chemical, and biological properties of ZnO, ZCE, and ZPL were investigated using a range of characterization techniques. A UV-visible (UV-vis) spectrophotometer with a wavelength range of 200-600 nm was used to determine the synthesis of ZnO, ZCE, and ZPL. The crystalline nature and purity of NPs were investigated using an X-ray diffractogram (XRD). SEM was employed to ascertain the shape of the particles, and energy dispersive spectroscopy was employed to validate their elemental composition (EDS). Furthermore, Fourier transform infrared spectroscopy (FTIR) was engaged to validate the production of ZnO, ZCE, and ZPL. The sample was scanned in the 400-4000 cm^{-1} spectral

region. TG/DTA measurements were performed using a TA Instruments Q600SDT TG/DTA in a nitrogen atmosphere at a heating rate of 10°C/min over the temperature range of 25–700°C. The mechanical behavior of the samples was assessed by compression and tensile tests using an Instron 5900, dry specimens.

2.5. Estimation of antibacterial activity by the well diffusion method.

The bactericidal capability of ZnO, ZCE, and ZPL was tested in nutritional agar using the well diffusion technique [21]. The following is a brief explanation of the approach used to assess the antibacterial activity. By using the well diffusion methodology on nutrient agar, the investigated material's antibacterial activity was evaluated. The bacterial strains *E. coli* (ATCC 10536) and *S. aureus* (ATCC 25923) were used as references for the antibacterial assay. A bacterial strain was injected into nutrient Agar plates in an aseptic environment, and the plates were spread-plated with a glass L-rod that contained 100 µL of growing culture. Then, a round (9 mm) aseptically stainless-steel bunching cork is used to make the well for each plate, and different concentration (25–100 µL) of the antimicrobial agent solution is introduced into the well. The next step was a 24-hour incubation period at 37°C. The zone of inhibition was measured and reported in millimeters (mm) after incubation. The concentration, known as the minimum inhibitory concentration (MIC), inhibited the growth of the particular microorganisms. Each assay was conducted three times. 100 µL of chloramphenicol dissolved in distilled water was used as the control.

2.6. Estimation of antifungal activity by the well diffusion method.

Agar was autoclaved together with the YPD Broth (YEPD Broth) medium. The sterile medium was used to cultivate the fungal cells for a whole night at 37°C. The autoclaved YEPD Broth agar was plated and left to cool on a standard petri dish. Following the solidification of the agar, 100 µL of each strain of *Aspergillus niger* (ATCC 1015) and *Candida albicans* (ATCC 90028) were spread-plated onto the YEPD Broth agar plates using an L-rod. By applying a sterile well cutter, holes were made in the agar plate. Each well was filled with varying concentrations of dissolved materials (25–100 µL). Following that, plates were incubated in environments that were suitable for the test microorganism. The zone of inhibition and the antibacterial activity of the provided samples were checked, and the plate pictures are shown below. The zone of inhibition was measured and presented in mm following the incubation time. Every assay was run in triplicate. The extracts were dissolved in distilled water and compared with 100 µL fluconazole as a control.

2.7. Evaluation of anticancer activity by MTT assay.

The monolayer cell culture was trypsinized, and the cell count was modified to 1.0 x 10^5 cells/ml using the appropriate medium containing 10% FBS. One hundred and fifty cells per well, or 100 µl of the diluted cell suspension, were added to each of the 96 microtiter plate wells. After 24 hours, when a partial monolayer had formed, 100 µL of different test drug doses was added to the partial monolayer in microtiter plates; the supernatant was discarded, and the monolayer was washed once more with medium. After that, the plates were incubated for 24 hours at 37°C in a setting with 5% CO_2. After the incubation period, the test solutions in each well were discarded, and 100 µL of MTT (5 mg/10 mL in PBS) was added. For four hours, the plates were incubated at 37°C with 5% CO_2. The formazan that had developed was dissolved

by gently shaking the plates after 100 µL of DMSO was added, and the supernatant was removed. A microplate reader was used to determine the absorbance at a wavelength of 590 nm. The percentage of growth inhibition was calculated using the following formula, and the concentration of the test medication required to block cell growth by 50% (IC50) was determined from dose-response curves for each cell line.

$$\% \text{ Inhibition} = 100 - \left[\frac{OD\ of\ sample}{OD\ of\ control}\right] x\ 100 \qquad \text{Eq(1)}$$

2.8. Statistical evaluation and IC_{50} Value determination.

When a compound is used to hinder biological or biochemical activity, its efficacy is measured by its half maximum inhibitory concentration (IC_{50}). This countable data shows the quantity of a precise medicine or other inhibitor substance obligatory to halve the inhibition of a given biological phenomenon (or process constituent, such as an enzyme, cell, cell receptor, or microbe). By creating a dose-response curve and scrutinizing the consequence of different antagonist concentrations in reversing agonist activity, one can discover a drug's half-life (IC_{50}). The concentration essential to impede half of an antagonist's maximal biological reaction can be used to compute the antagonist's IC_{50} values. Graph Pad Prism 6 (Graph Pad, SanDiego, CA, USA) was used to compute the IC_{50} data for cytotoxicity tests, which were obtained by a nonlinear regression analysis (curve fit) dependent on the sigmoid dosage response curve (variable).

2.9. Assessment of antioxidant activity by DPPH assay.

The DPPH radical is deep violet in solution, but when ZCE and ZPV are present, it gradually fades to colorless or light yellow. Samples' antioxidant activity was assessed through the application of the DPPH method with certain modifications. There was a 0.1 mM DPPH solution in methanol. Three milliliters of the sample solution in methanol, at concentrations ranging from 0.75 to 48 g/mL, were mixed with one milliliter of the same solution using a double-dilution method. After shaking the mixture vigorously, it was left to remain at room temperature for 30 minutes in the dark. A spectrophotometer was used to measure the absorbance at 517 nm after 30 minutes. A control response was carried out in the absence of the test sample. An increase in DPPH radical scavenging activity is suggested by a diminution in DPPH solution absorbance. Using the following formula, the percentage of DPPH's radical scavenging activity was estimated: The formula for calculating the percentage of radical scavenging activity is [(Ac-As)/Ac], where Ac and As represent the absorbances of the sample and control, respectively. Ascorbic acid served as the reference standard.

2.10. Theoretical molecular Docking Studies.

One straightforward theoretical method for assessing how well our synthesized substances bind to biomolecules is molecular docking. Mercury V3.6 was used to transform the molecular structures of ZCE and ZPL into mol files. The Gaussian 09 computational suite was used to optimize the mol files of samples using the LanL2DZ basis set. The Autodock vina program was used to conduct the docking investigations, and its tools were used.

3. Results and Discussion

3.1. XRD analysis.

XRD examination provided crystallographic information by identification of the phases associated with ZnO, ZCE, and ZPL samples, as represented in Figure 1. The 2θ values at 31.4°, 33.4°, 47.01°, 57.89°, 61.08°, 65.03°, 69.02°, 72.07° and 76.03° are correlated to (100), (002), (101), (102), (110), (103), (200), (112), (201), (004) and (202) planes of ZnO NPs as assigned by JCPDS file no. 361451. This characteristic pattern of peaks for ZnO existed in the XRD of as-synthesized ZnO NP, as noted from Figure 1a. However, a few peaks are modified from their position. In the XRD pattern of ZCE and ZPL, a broader prominent peak at around 19.6°, characterizes the presence of semi-crystalline polymer.

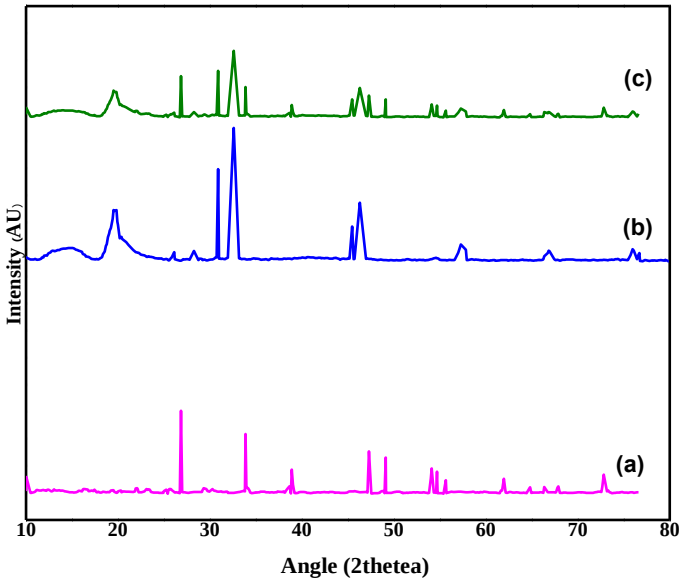

Figure 1. Powder XRD pattern of biosynthesized **(a)** ZnO; **(b)** ZCE; **(c)** ZPL.

The typical peaks of the polymer appeared at 10.67° and 18.99°, while these peaks became weaker in the XRD pattern, indicating that incorporation of the polymer into ZnO results in a change in the degree of crystallinity. From Figures 1b and 1c, we can infer that both the peaks related to the polymeric region (organic phase) and ZnO (inorganic phase) are present. All the recorded peak intensities were characteristic of the hexagonal wurtzite ZnO structure [22,23]. It can be observed that the signals are due to the 200 and 220 planes, which were low and feeble in the XRD of ZCE and ZPL. These data indicate that the peaks of polymer-incorporated ZnO are less intense and wider than those of pure ZnO.

3.2. SEM analysis.

SEM images of ZnO, ZCE, and ZPL samples collected at different magnifications are shown in Figures 2, 3, and 4 (a-d), respectively. The SEM picture of pristine ZnO in Figure 2 shows that particle agglomeration was substantially higher, and the particles exhibit an uneven-sized morphology. By contrast, after incorporating polymers, the extent of agglomeration has been decreased, as evident from Figures 3 and 4. ZnO particles are not visible, but the particle agglomeration is slightly deformed in ZCE and ZPL samples.

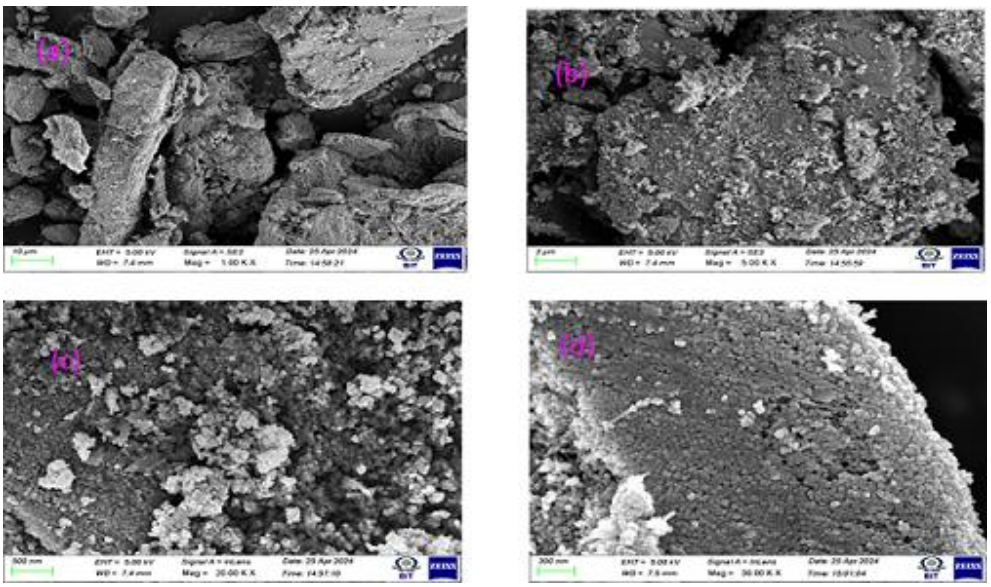

Figure 2. SEM images of ZnO under different magnifications of 10 µ, 2 µ, 500 nm, and 200 nm.

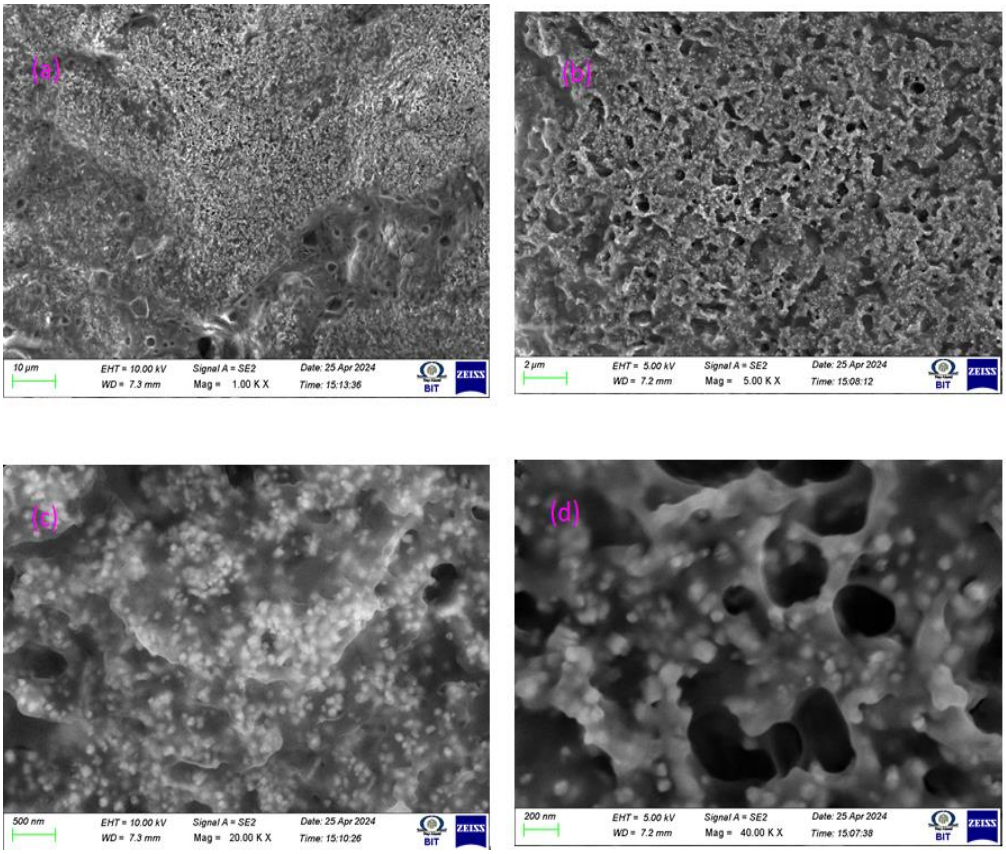

Figure 3. SEM images of ZCE under different magnifications of 10 µ, 2 µ, 500 nm, and 200 nm.

A spherical structure was observed in ZCE and ZPL samples; higher-magnification images showed an accretion of a group of tiny spherical particles, ranging from 20 to 60 nm, collectively forming a cluster-like structure with a diameter of 300-400 nm. From these images, it can be deduced that as the extent of particle agglomeration decreases, the surface area is enhanced after incorporating a polymer with ZnO. Figure 5 (a,b,c) shows the EDS patterns of ZnO, ZCE, and ZPL samples, respectively.

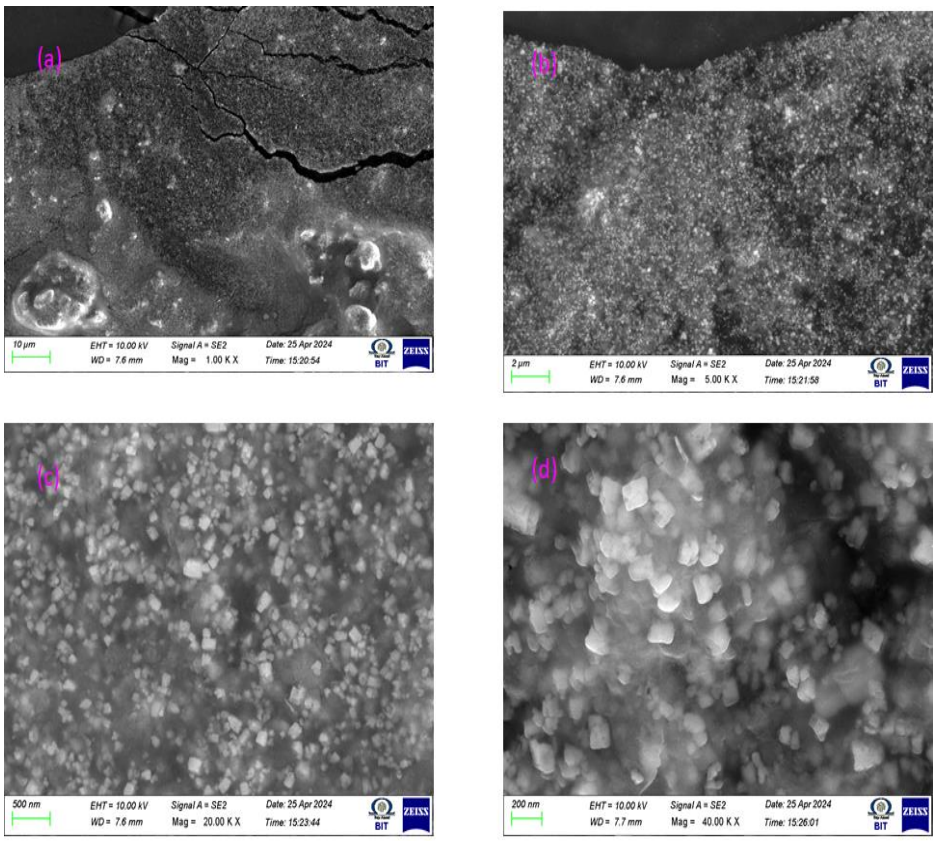

Figure 4. SEM images of ZPL under different magnifications of 10 µ, 2 µ, 500 nm, and 200 nm.

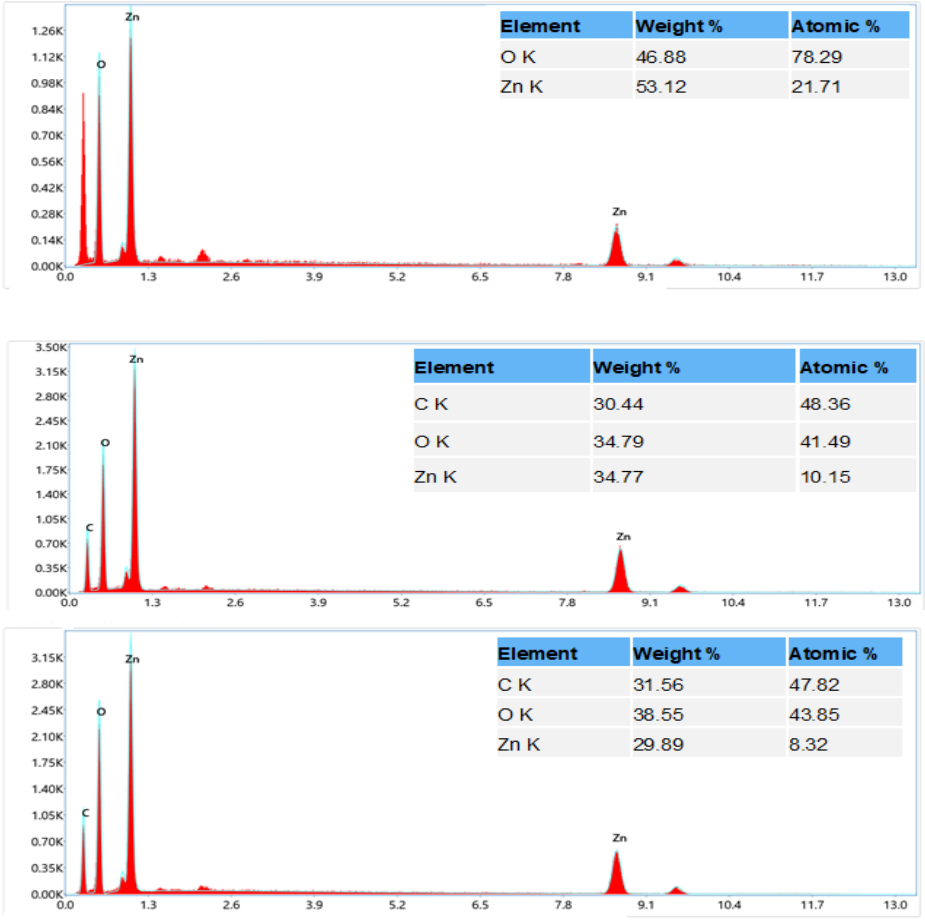

Figure 5. The EDX spectra of **(a)** ZnO; **(b)** ZCE; **(c)** ZPL.

The presence of zinc, carbon, and oxygen components in the ZCE and ZPL of the samples indicates interaction between ZnO and the polymers; however, EDS of ZnO showed only zinc and oxygen.

3.3. FTIR analysis.

Figure 6 displays the FTIR spectra of synthesized ZnO, ZCE, and ZPL samples. The high-intensity band at 434 cm^{-1} was attributed to Zn-O stretching vibration, which is modified when the polymer is blended with ZnO. The peaks appeared at 562 cm^{-1}, 650 cm^{-1}, 779 cm^{-1}, 927 cm^{-1}, 1141 cm^{-1}, 1567 cm^{-1}, 1644 cm^{-1}, 2143 cm^{-1}, 2853 cm^{-1}, 2922 cm^{-1}, and 3432 cm^{-1}, which designate the specified functional group existing in the synthesized zinc oxide nanoparticles and are in accordance with the previous literature [24,25]. It is conjectured that the sample's absorption peaks occur in the range of 434 to 575 cm^{-1}, associated with the metal-oxygen (ZnO stretching vibration) mode. FTIR spectra of both ZCE and ZPL nanocomposites are encompassed with distinct peaks of ZnO NP, a few of which are shifted towards higher frequency with altered intensity. Nevertheless, features of both ZnO NPs and the polymeric component have been observed in the spectrum of the ZCE and ZPL nanocomposite.

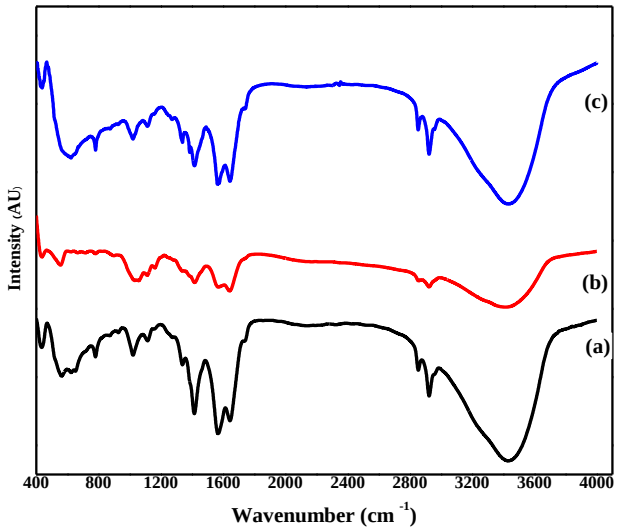

Figure 6. FTIR spectra for biosynthesized **(a)** ZnO; **(b)** ZCE; **(c)** ZPL.

FTIR spectrum obtained for the ZCE sample disclosed a low-intensity band at 3490 cm^{-1}, attributed to O-H stretching vibrations, and a characteristic band at 897.95 cm^{-1}, which is the glycosidic bond β-(1→4) present in the cellulose, is noticeable. Besides, the C-H stretching vibration is noticed at 2924 cm^{-1}. Additionally, a band observed at approximately 1641 cm^{-1} is indicative of the unconjugated hemicellulose C=O stretching, while the peak at 2922 cm^{-1} corresponds to the asymmetrical stretching of CH_2 and CH, which signifies the presence of cellulose [26]. The spectral region spanning from 3800 cm^{-1} to 3000 cm^{-1} reflects the crystalline nature of cellulose structure. This range encompasses the collective vibrations of the valence bands associated with the hydrogen bonds of the O-H group, as well as those associated with both intra- and inter-molecular hydrogen bonding.

Similarly, incorporation of polyvinyl alcohol into ZnO has significantly reformed the FTIR spectrum of ZPL. Owing to the presence of ZnO, the width of bands corresponding to -CH_2 and -OH groups has become lowered in intensity. The ZPL spectrum shows typical O-H stretching at about 3437 cm^{-1}, C-O stretching at around 1020 cm^{-1}, and asymmetric CH_2 stretching at around 2922 cm^{-1}, indicating the formation of bonding interactions between the

functional groups of polyvinyl alcohol and ZnO [27]. The absorption peaks. Hydrogen-bonding and new electrostatic interactions form between ZnO and polymers, as evidenced by the spectra. The examination of the FTIR spectra of the synthesized polymers relative to those of ZnO NPs indicates that most bands are well-defined, with minimal variation in both intensity and frequency. Such discrepancies in the absorption bands' intensities and frequencies can be attributed to bond formation between the ZnO NP and the polymer.

3.4. UV visible spectroscopy.

The UV–vis spectroscopy of biosynthesized ZnO, ZCE, and ZPL in the wavelength range of 200–800 nm is shown in Figure 7. The absorption band at 370 nm is due to electron transport from the valence band to the conduction band.

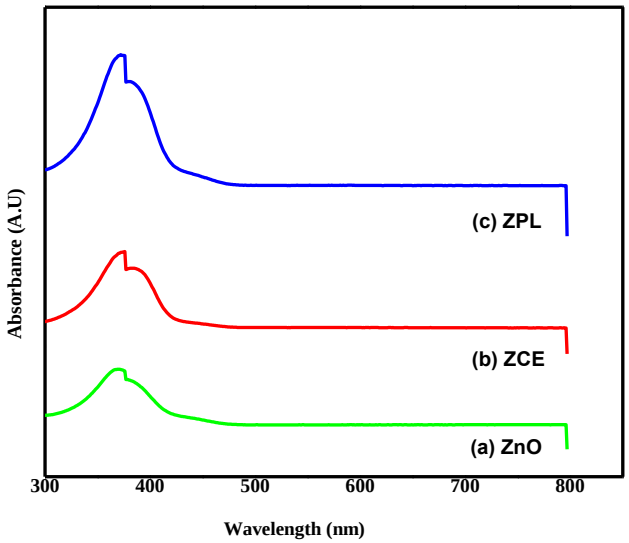

Figure 7. UV-Vis spectra for biosynthesised **(a)** ZnO; **(b)** ZCE; **(c)** ZPL.

An observable sharp peak at 370 nm confirmed the presence of ZnO NPs in the polymeric composites, also [28]. The broader absorption shifting towards lower wavelength might be owing to the movement of the electronic cloud in the overall outer region of the ZnO NPs. After incorporating the polymer, the peak at 370 nm shifts to 362 nm and 366 nm for ZCE and ZPL, respectively, indicating a distinctive interaction between the polymer and ZnO NPs. Both cellulose and polyvinyl alcohol contain alcoholic groups; hence, these functional groups can interact with ZnO NPs via hydrogen bonding and electrostatic attraction. This observation, at another time, demonstrates the upright interaction between the polymer components and ZnO NPs.

3.5 Thermogravimetric analysis.

The thermo-gravimetric investigation of ZnO, ZCE, and ZPL has been analyzed using TGA, as designated by Figure 8. The thermal degradation pattern proceeds in stages, with the first stage in all three samples showing the lowest weight loss, which has been linked to the loss of solvent molecules. Nearly 95% of the water molecules have been eliminated at this early initial stage of temperature (100–120°C). Beyond 200°C, the second step of weight loss has occurred; whereas, at this temperature, the polymers begin to break down [29,30]. Along with structural degradation, this stage is characterized by the breakup of the polymeric chain and a slight decrease in weight below 300 °C, which is probably due to partial polymer degradation.

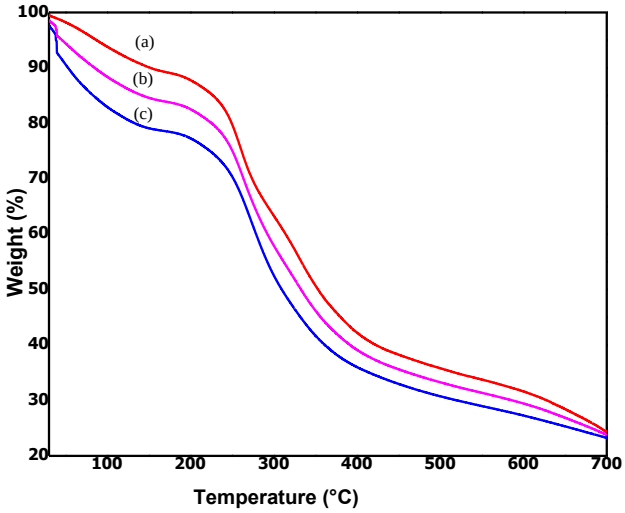

Figure 8. Thermogravimetric analysis associated with **(a)** ZnO; **(b)** ZCE; **(c)** ZPL.

The results revealed that the presence of the polymer influenced the thermal curve to a lower temperature. The residual final deposit of metal oxide is thought to have resulted from the metal complex's basic decomposition at higher temperatures. These investigations indicate that the addition of polymers changed the thermal characteristics of ZnO.

3.6. Mechanical properties.

Mechanical properties of ZnO, ZCE, and ZPL have been analyzed using compression tests of samples; sufficient mechanical stability is a prime requirement for structural integrity and stability, as shown in Figure 9.

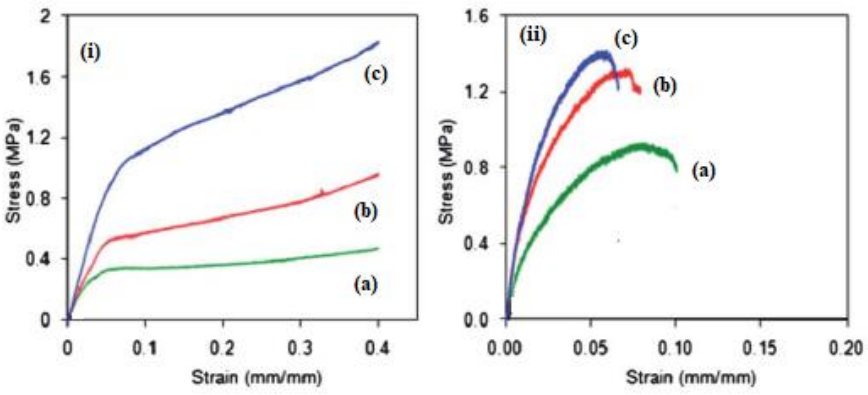

Figure 9. Mechanical properties of **(a)** ZnO; **(c)** ZPL; **(b)** ZCE samples. Stress-strain dependence of samples obtained in **(i)** compression test; **(ii)** tensile test.

Upon integration with the polymer, ZnO displayed a pronounced enhancement in mechanical properties; ZCL possessed 3 times higher strength in comparison to ZnO. The increase in stability is due to closer packing and favorable interaction between ZnO and the polymer.

3.7. Biological activities.

3.7.1. Antimicrobial activity.

The biological activities of ZCE and ZPL are evaluated through antibacterial, antifungal, antioxidant, and anticancer activities. The results, as shown in Figure 10, indicated

that the rate of inhibition depends on concentration; inhibitory activity was higher at higher concentrations, as evident from Table 1. Besides, it is notable that the growth of *E. coli* is well-inhibited by ZCE, while ZPE is more efficient towards inhibiting *S. aureus*. The difference in the activity is attributed to differences in the (i) mode of action, (ii) chemical constitution, and (iii) particle size. It has been anticipated that positively charged Zn^{2+} ions might be intermingled with bacteria *via* electrostatic interactions, hindering enzyme production and deactivating DNA by interacting with the oppositely charged components of the bacterial cell wall, which eventually results in cell death [31,32].

The study shows that ZCE and ZPL can help develop new treatments for diseases caused by harmful bacteria due to their effectiveness.

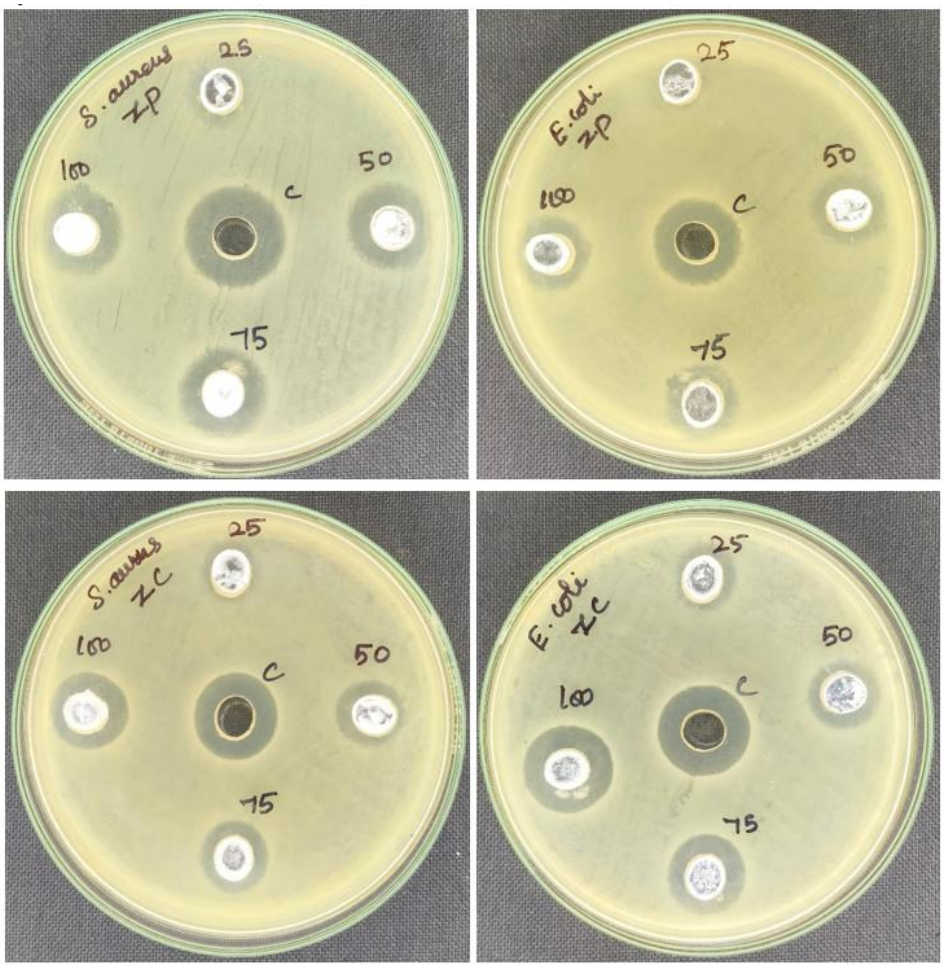

Figure 10. Antibacterial activity of biosynthesized ZCE and ZPL towards **(a)** *Staphylococcus aureus*; **(b)** *Escherichia coli.*

The nanocomposite of dopamine-coated zinc oxide exhibited notable zones of inhibition (ZOI) of 11.56 mm for *B. cereus* and 11.80 mm for *E. coli*, respectively, highlighting its broad-spectrum antimicrobial potential [33]. The highest inhibition zone (14 and 15 mm) was observed at the ratios of 4 and 6 wt.% of ZnO NPs against *E. coli*, which was reported for PVA-PVP/ZnO nanofiber films prepared *via* indigenous electrospinning [34]. Similar results are observed in this study, also.

It is apparent that the size, shape, and biosynthetic composition are the three key factors that significantly stimulate microbial activity. They exhibit maximum antibacterial activity, which can be attributed to both the surface-capping properties of the phytochemicals and their small particle size.

Similarly, antifungal activity was assessed using Fluconazole as a standard drug, and the zone of inhibition is depicted in Figure 11; the related data are provided in Table 2. ZCE and ZPL were successfully evaluated for their *in vitro* studies against *Candida albicans* and *Aspergillus niger*. It is remarkable that both ZCE and ZPL were found to be discreetly active at lower concentrations but showed significant activity when tested at higher concentrations. With respect to *Aspergillus niger*, equally good activity was shown by both ZCE and ZPL.

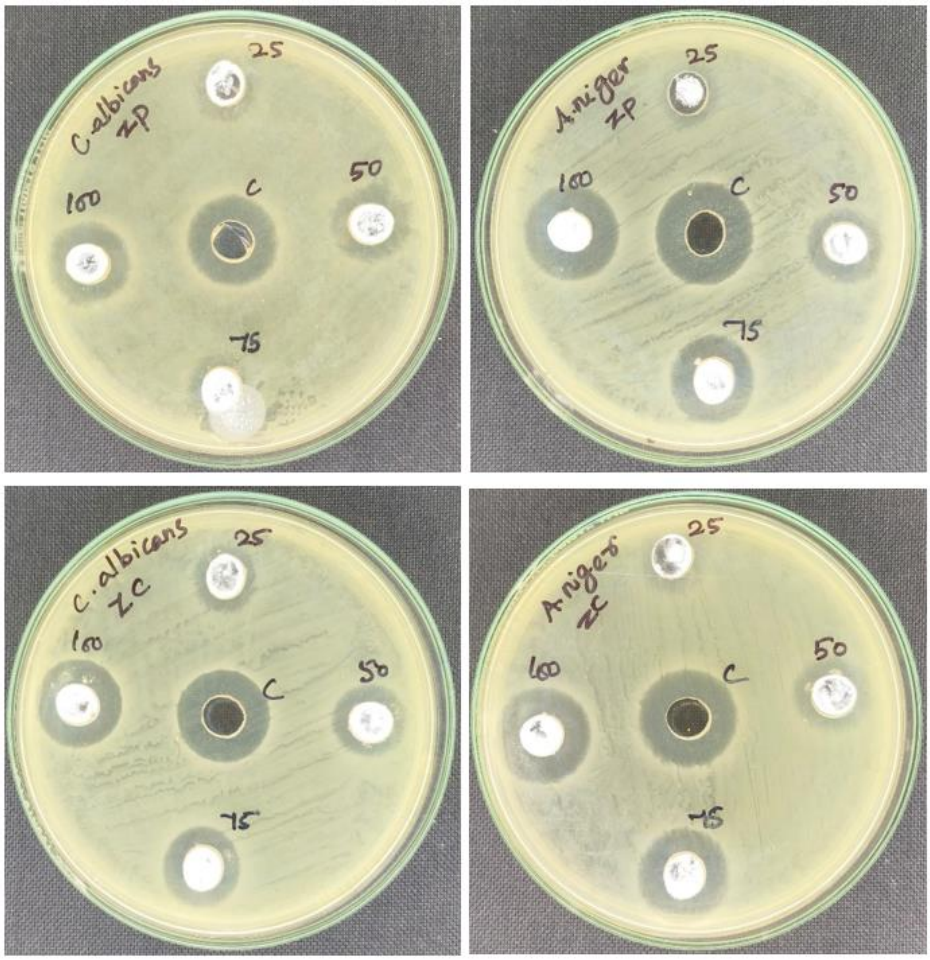

Figure 11. Antifungal activity of biosynthesized ZCE and ZPL towards **(a)** *Staphylococcus aureus*; **(b)** *Escherichia coli.*

With *Candida albicans* fungal strains, appreciable activity was notable at higher concentrations. The presence of the positively charged metal ion may be accountable for the antifungal activity of these compounds, as it reduces electron cloud density and facilitates access to target molecules in fungal cells [35,36]. The degree to which different biocidal chemicals are effective against different species depends on the cells' permeability. The mechanism of action proceeds in steps: it impairs cell permeability, inhibits cell wall synthesis, and then mitigates cellular respiration, destroying active cellular constituents and effectively killing the microorganisms.

3.7.2. Antioxidant activity.

Free radical or oxidative damage is one of the primary reasons for the repair of internal organs and tissues. Figure 12 demonstrates the antioxidant activities of ZCE and ZPL samples (DPPH free radical scavenging).

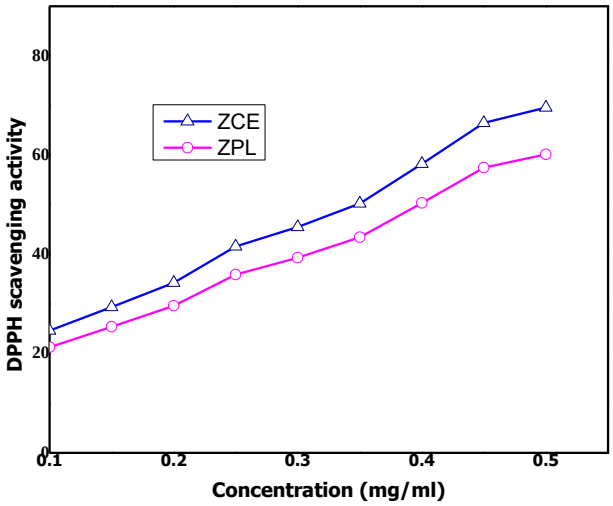

Figure 12. Demonstrates the antioxidant activities of ZCE and ZPL samples towards DPPH free radical scavenging.

The compounds based on antioxidants must therefore be produced synthetically. The antioxidant experiments were carried out at concentrations ranging from 0.1 to 0.5 mg/mL. For the ZCE and ZPL samples, the maximum total antioxidant values were 69.6% and 60.9%, respectively, at higher concentrations. The study shows that the polymer protects the body by binding with metal ions, with IC_{50} values of 0.34 and 0.39 mg/mL for ZCE and ZPL, respectively. Similar results were reported for diverse ZnO composites. Almond gum-capped green-synthesized ZnO was shown to exhibit good anticancer activity against the colon cancer cell line (HT-29), resulting in a significant reduction in cell proliferation after 24 h, with an IC_{50} of 30.69 µg/ml [37]. Gelatin-coated ZnO displayed anticancer activity against the HT-29 cell line, with an IC50 of 45.4 µg/mL, as reported in a recent study [38].

3.7.3. Antiproliferative activity.

In the present analysis, we scrutinized the cytotoxicity effect of synthesized ZCE and ZPL nanocomposites on breast cancer cells (MDA-MB-231). The results are presented in Figures 13 and 14, respectively.

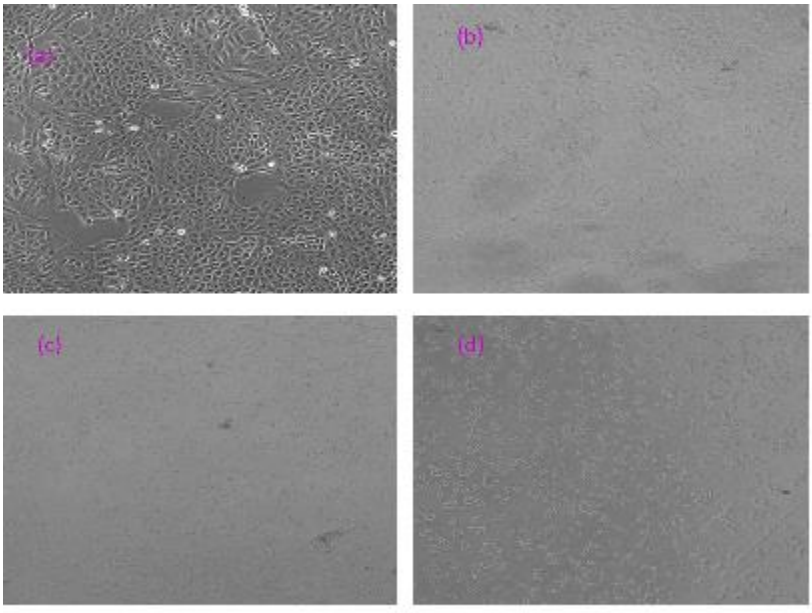

Figure 13. The cytotoxicity effect of ZCE nanocomposite towards the HT-29 human colon cancer cell line.

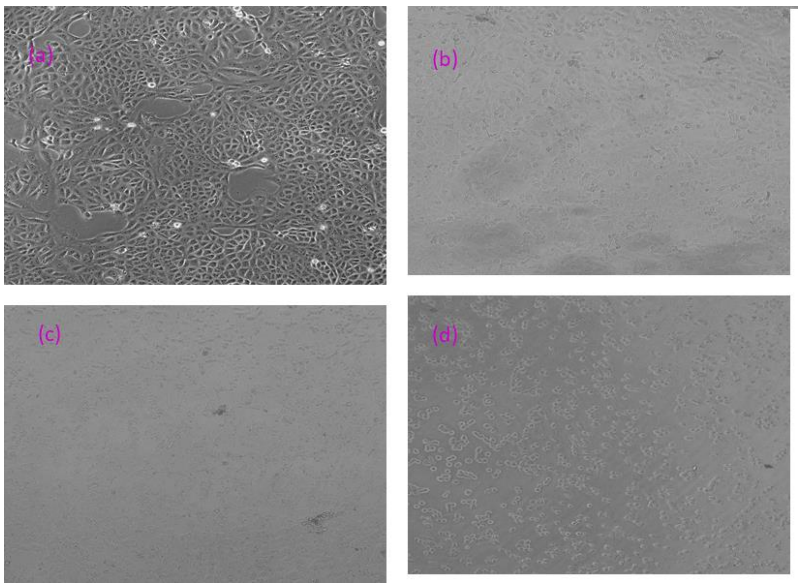

Figure 14. The cytotoxicity effect of ZPL nanocomposite towards the HT-29 human colon cancer cell line.

The findings show that while an increase in concentration has a considerable toxic impact, both nanocomposites exhibit nearly identical toxicity effects. Certain reports suggested that ZnO particles are selectively harmful to bacteria, whereas other reports proposed that ZnO particles can induce cytotoxicity via mechanisms including necrosis, apoptosis, and genotoxicity, which are thought to involve radicals. According to earlier observations [39-41], the cytotoxicity action requires direct particle-cell interaction, followed by specific uptake, resulting in the release of Zn2+ ions into intracellular concentrations that are rapidly dissolved within lysosomes or late endosomes. Particle size and shape, concentration, and dispersion state are some of the variables that affect toxicity. We anticipate that the polymeric coating alters ZnO's specific surface area, dissolution rate, and absorption mechanism, resulting in reduced toxicity and making it suitable for biological applications. As a result, our data on cell viability indicate that adding cellulose or polyvinyl alcohol to ZnO NPs decreases their cytotoxicity to human cells. This effect is attributed to both the polymer's presence and the particles' increased size. This is consistent with earlier research that found ZnO NPs coated with polymers have less cytotoxicity. As the concentration increased, observations showed that the cytotoxic effect became more pronounced and reached statistical significance at 50 µg/mL. Since ZCE's cytotoxic effect was comparatively greater than ZPL's, it may be concluded that cellulose's presence induced cytotoxicity. ZCE and ZPL had inhibitory concentrations (IC_{50}) of 44.7 ± 0.05 µg/mL and 51.53 ± 0.05 µg/mL, respectively, according to MTT assay results. Since ZCE has a lower IC_{50} (44.7 µg/mL) than ZPL (51.53 µg/mL), it suggests that ZCE is more potent or effective at inhibiting the cells being tested in the MTT assay compared to ZPL.

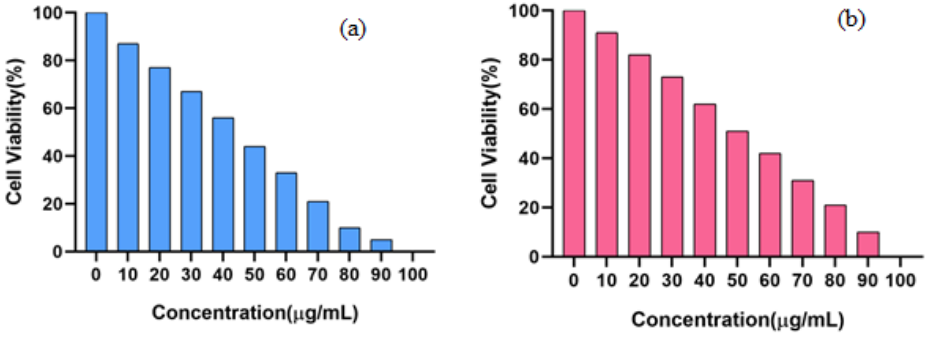

Figure 15. The graph demonstrating the IC_{50} value of the MMT assay for **(a)** ZCE; **(b)** ZPL.

3.7.4. Molecular docking with BSA protein and DNA molecules.

Both ZCE and ZPL samples are docked with the BSA protein (PDB ID: 3V03) molecule using the Autodockvina program. ZCE and ZPL samples interact with the dual-chained molecule by attaching to definite amino acid targets; hence, the interactive binding energy values are determined by both the nature of the interacting molecule and the biomolecule with which it is attached. The docking images were provided in Figure 16. It can offer details regarding:

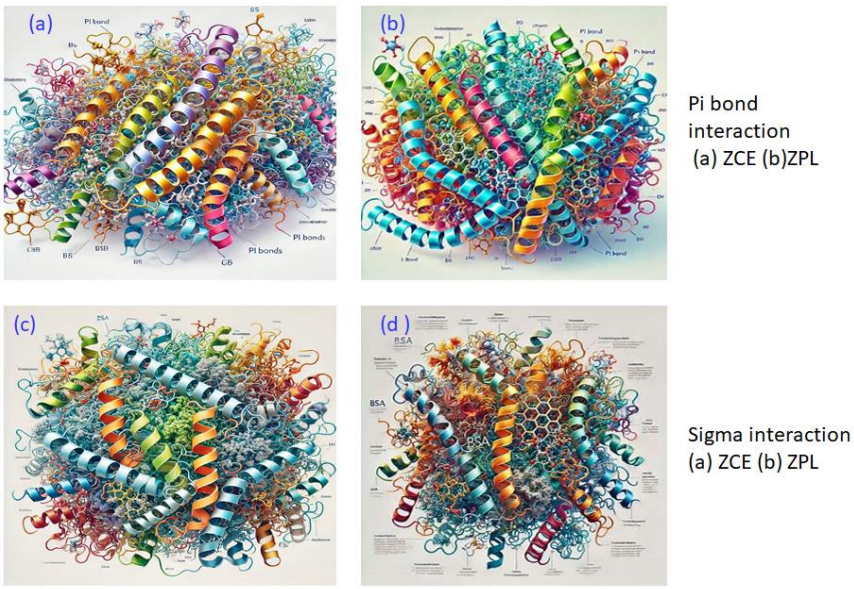

Figure 16. The molecular docking studies for **(a)** ZCE; **(b)** ZPL.

The binding location, the ligand's configuration, the ligand's affinity for the protein, the quantity of binding sites, and the binding mechanism [42, 43]. ZCE displayed a binding energy value of 12.3 kcal/mol, whereas ZPL showed only 11.8 kcal/mol, illustrating greater binding affinity of ZCE, which possesses interaction with ARG427, ILE522, ARG427, and PRO420 using pi-sigma. Nonetheless, ZPL interacted with ARG427, PRO420, and ARG458 through pi-pi and pi-sigma interactions. The interaction images and the bond distance value were noted in Table 1. Docking studies contribute to lead optimization by guiding structural modifications to enhance a compound's binding to the target, potentially increasing its efficacy and selectivity. Molecular docking studies can provide insights into the anticancer activity of compounds demonstrated in in vitro and in vivo studies.

4. Conclusions

In this study, ZnO nanoparticles were synthesized with the use of aqueous *Calotropis gigantea* flower bio extract. The reducing activity of the bioextract was synergistically enhanced by the microwave process, which influenced the shape and particle morphology. The synthetic process method detailed in this document marks a significant step forward in the green synthesis of metal nanoparticles. The nanoparticles are combined with polymers, namely cellulose and polyvinyl alcohol, to produce nanocomposites that are characterized spectrally by UV–vis, FTIR, XRD, SEM, and EDX analyses. The antibacterial activity was evaluated against two bacterial strains, *S. aureus* and *E. coli*, as well as two fungal strains, *C. albicans* and *A. niger*. As the concentration increased, cytotoxic effects became more evident, reaching statistical significance at 50 µg/mL. According to the results of the MTT assay, ZCE and ZPL

demonstrated inhibitory concentrations (IC_{50}) of 44.7 ± 0.05 µg/mL and 51.53 ± 0.05 µg/mL, respectively. Molecular docking studies with BSA protein reveal the potential of the materials as prodrugs for cancer treatment, with future considerations aimed at enhancing their effectiveness. In summary, the nanocomposites prepared show considerable promise for various biomedical applications, including antibacterial, antioxidant, and anticancer properties.

Author Contributions

Conceptualization, K.K.; formal analysis, K.K.; methodology, G.D.K.; data curation, G.D.K.; writing—original draft preparation, G.K.; writing—review and editing, G.K.; supervision, G.K.; investigation, G.K.; software, S.M.; validation, S.M.; resources, S.M. All authors have read and agreed to the published version of the manuscript.

Institutional Review Board Statement

Not applicable.

Informed Consent Statement

Not applicable.

Data Availability Statement

Data supporting the findings of this study are available upon reasonable request from the corresponding author.

Funding

No external funding was received for this work.

Acknowledgments

Declared none.

Conflicts of Interest

All authors declare no competing interests.

References

1. Gadewar, M.; Prashanth, G.K.; Babu, M.R.; Dileep, M.S.; Prashanth, P.A.; Rao, S.; Mahadevaswamy, M.; Ghosh, M.K.; Singh, N.; Mandotra, S.K.; Chauhan, A. Unlocking nature's potential: Green synthesis of ZnO nanoparticles and their multifaceted applications–A concise overview. *J. Saudi Chem. Soc.* **2024**, *28*, 101774, https://doi.org/10.1016/j.jscs.2023.101774.
2. Thirumavalavan, M.; Sukumar, K.; Sabarimuthu, S.Q. Trends in green synthesis, pharmaceutical and medical applications of nano ZnO: A review. *Inorg. Chem. Commun.* **2024,** *169*, 113002, https://doi.org/10.1016/j.inoche.2024.113002.
3. Al-darwesh, M.Y.; Ibrahim, S.S.; Mohammed, M.A. A review on plant extract mediated green synthesis of zinc oxide nanoparticles and their biomedical applications. *Results Chem.* **2024**, *7*, 101368, https://doi.org/10.1016/j.rechem.2024.101368.
4. Soni, J.; Revathi, D.; Dhanraj, G.; Ramasubburayan, R. Bioinspired green synthesis of ZnO nanoparticles by marine-derived Streptomyces plicatus and its multifaceted biomedicinal properties. *Microbial Pathogenesis* **2024**, *193*, 106758, https://doi.org/10.1016/j.micpath.2024.106758.

5. Mongy, Y.; Shalaby, T. Green synthesis of zinc oxide nanoparticles using Rhus coriaria extract and their anticancer activity against triple-negative breast cancer cells. *Sci. Rep.* **2024**, *14*, 13470, https://doi.org/10.5281/zenodo.8329357.
6. Alalawy, A.I.; Saleh, F.M.; Saeedi, N.H.; Panneerselvam, C.; Sakran, M.I.; Khasim, S.; Parveen, H.; Mohammedsaleh, Z.M.; Mukhtar, S.; Faridi, U.; Alasmari, A. Green synthesis of Bb-ZnO NPs using Barleria buxifolia leaf extract: Investigations into their physicochemical, biological and anti-cancer properties. *Polyhedron* **2025**, *267*, 117366, https://doi.org/10.1016/j.poly.2024.117366.
7. Vieira, I.R.; da Silva, A.A.; da Silva, B.D.; Torres Neto, L.; Tessaro, L.; Lima, A.K.; Garcia, M.P.; Ribeiro, J.A.; Rodrigues, C.M.; de Sousa, A.M.; Carvalho, N.M. Antioxidant, antimicrobial, and anticancer potential of green synthesized ZnO nanoparticles from Açaí (euterpe oleracea mart.) berry seed residue extract. *Waste Biomass Valorization* **2024**, *15*, 4717-4734, https://doi.org/10.1007/s12649-024-02485-5.
8. Irede, E.L.; Awoyemi, R.F.; Owolabi, B.; Aworinde, O.R.; Kajola, R.O.; Hazeez, A.; Raji, A.A.; Ganiyu, L.O.; Onukwuli, C.O.; Onivefu, A.P.; Ifijen, I.H. Cutting-edge developments in zinc oxide nanoparticles: synthesis and applications for enhanced antimicrobial and UV protection in healthcare solutions. *RSC Adv.* **2024**, *14*, 20992-21034, https://doi.org/10.1039/D4RA02452D.
9. Asif, N.; Amir, M.; Fatma, T. Recent advances in the synthesis, characterization and biomedical applications of zinc oxide nanoparticles. *Bioprocess Biosyst. Eng.* **2023**, *46*, 1377-1398, https://doi.org/10.1007/s00449-023-02886-1.
10. Qu, B.; Xiao, Z.; Luo, Y. Sustainable Nanotechnology for Food Preservation: Synthesis, Mechanisms, and Applications of Zinc Oxide Nanoparticles. *J. Agric. Food Res.* **2025**, *19*, 101743, https://doi.org/10.1016/j.jafr.2025.101743.
11. Al-Hamadani, N.H.; Pouresmaeil, V.; Sharbatiyan, M.; Homayouni Tabrizi, M. Investigation into the anticancer activity of biosynthesized zinc oxide nanoparticles incorporating 6-gingerols. *Cell. Mol. Biomed. Rep*. **2025**, *5*, 168-186, https://doi.org/10.55705/cmbr.2025.495731.1296.
12. Bhushan, S.; Singh, S.; Maiti, T.K.; Das, A.; Barui, A.; Chaudhari, L.R.; Joshi, M.G.; Dutt, D. Zinc-doped hydroxyapatite loaded chitosan gelatin nanocomposite scaffolds as a promising platform for bone regeneration. *Biomed. Mater*. **2025**, *20*, 025006, https://doi.org/10.1088/1748-605X/ada477.
13. Ieamviteevanich, P.; Onklam, P.; Kampechdee, W.; Churiwan, A.; Vittayakorn, N.; Prachayawarakorn, J.; Seeharaj, P. Asymmetric dot-patterned wettable and antibacterial wound dressings from bacterial cellulose–alginate composites coated with stearic acid-modified ZnO/chitosan/AgNPs. *Cellulose* **2025**, *32*, 329-350, https://doi.org/10.1007/s10570-024-06278-w.
14. Alwadai, N. Investigation on structural, optical, thermal, and dielectric properties of nanocomposite films based on chitosan containing vanadium pentoxide/zinc oxide and their potential for optoelectronics devices. *J. Mol. Struct*. **2024**, *1312*, 138491, https://doi.org/10.1016/j.molstruc.2024.138491.
15. Alsolmi, M.M.; El-Naggar, N.E.-A.; Alqurashi, M.I.; Hamouda, R.A. Biofabrication of zinc oxide nanoparticles using Moringa oleifera, characterization and statistical optimization for their application in crystal violet adsorption. *Sci. Rep.* **2025**, *15*, 3780, https://doi.org/10.1038/s41598-025-86629-0.
16. Qanash, H.; Bazaid, A.S.; Alharbi, S.F.; Binsaleh, N.K.; Barnawi, H.; Alharbi, B.; Alsolami, A.; Almashjary, M.N. Therapeutic Effects of Nanocoating of Apitoxin (Bee Venom) and Polyvinyl Alcohol Supplemented with Zinc Oxide Nanoparticles. *Pharmaceutics* **2025**, *17*, 172, https://doi.org/10.3390/pharmaceutics17020172.
17. Badry, R.; Sabry, N.M.; Ibrahim, M.A. Enhancing the structural and optoelectronic properties of carboxymethyl cellulose sodium filled with ZnO/GO and CuO/GO nanocomposites for antimicrobial packaging applications. *Sci. Rep.* **2024**, *14*, 30591, https://doi.org/10.1038/s41598-024-81365-3.
18. Karthik, P.; Ravichandran, S.; Prakash, N.; Mukkannan, A.; Rajesh, J. Evaluation of ZnO infused CA/PCL nanocomposites using potential wastewater treatment and invitro anticancer activity. *Water Cycle* **2024**, *5*, 121-130, https://doi.org/10.1016/j.watcyc.2024.03.002.
19. Liu, Z.; Chen, X.; Ling, W.; Wang, M.; Qiu, B.; Shi, J. Synthesis of core–shell ZnO nanoparticles and their effect on mechanical and antibacterial properties for PLLA/ZnO nanocomposites. *Polym. Compos.* **2024**, *45*, 3448-3459, https://doi.org/10.1002/pc.28001.
20. de Sousa, A.L.; Rebouças, L.M.; Lemos, F.M.; Ribeiro, A.C.; Cunha, F.E.; Pessoa, C.; Sales, S.L.; Silva, L.M.; Ricardo, N.M. Nanoemulsion based on Calotropis procera seed oil to delivery of betulinic acid: In vitro release kinetics, in vivo toxicity and MTT assay in PC3 cells. *J. Drug Deliv. Sci. Technol.* **2025**, *106*, 106746, https://doi.org/10.1016/j.jddst.2025.106746.

21. Singh, N.K.; Khatiwada, N. Calotropis Procera Plant Extract: Phytochemical Analysis, Antimicrobial Activity, and Coumarin Compound Identification. *KMC J.* **2025**, *7*, 371-388, https://doi.org/10.3126/kmcj.v7i1.75161.
22. Albarakaty, F.M.; Alzaban, M.I.; Alharbi, N.K.; Bagrwan, F.S.; Abd El-Aziz, A.R.; Mahmoud, M.A. Zinc oxide nanoparticles, biosynthesis, characterization and their potent photocatalytic degradation, and antioxidant activities. *J. King Saud Univ. Sci.* **2023**, *35*, 102434, https://doi.org/10.1016/j.jksus.2022.102434.
23. Sani, A.; Hassan, D.; Ehsan, M.; Sánchez-Rodríguez, E.P.; Melo-Máximo, D.V. Improving strawberry shelf life using chitosan and zinc oxide nanoparticles from ginger-garlic extracts. *Appl. Food Res.* **2025**, *5*, 100765, https://doi.org/10.1016/j.afres.2025.100765.
24. Ramesh, P.; Rajendran, A.; Ashokkumar, M. Biosynthesis of zinc oxide nanoparticles from Phyllanthus Niruri plant extract for photocatalytic and antioxidant activities. *Int. J. Environ. Anal. Chem.* **2024**, *104*, 1561-1572, https://doi.org/10.1080/03067319.2022.2041004.
25. Okaiyeto, K.; Gigliobianco, M.R.; Di Martino, P. Biogenic zinc oxide nanoparticles as a promising antibacterial agent: synthesis and characterization. *Int. J. Mol. Sci.* **2024**, *25*, 9500, https://doi.org/10.3390/ijms25179500.
26. Penrasamee, S.; Than-ardna, B.; Charoensuk, S.; Manuspiya, H. Ferroelectric properties of functionalized metal and metal oxide nanoparticles embedded on bacterial cellulose films. *Cellulose* **2025**, *32*, 2451-2469, https://doi.org/10.1007/s10570-025-06419-9.
27. Luoyan, D.; Feiyi, Y.; Lei, Z.; Bo, L.; Yichi, Z.; Xinyuan, T.; Zhaoping, L.; Xiaodan, W.; Shuaiyu, W.; Jijing, T.; Huihui, B.; Tianlong, L.; ZnO@Polyvinyl Alcohol/Poly(lactic acid) Nanocomposite Films for the Extended Shelf Life of Pork by Efficient Antibacterial Adhesion. *ACS Omega* **2022,** 7, 44657. https://doi.org/10.1021/acsomega.2c03016.
28. Kalladi, A.J.; Ramesan, M. Green-Synthesized Zinc Oxide/Polyvinyl Alcohol/Cashew Gum/Polypyrrole Nanocomposites With Enhanced Mechanical, Thermal, and Electrical Properties for Nanoelectronics. *J. Appl. Polym. Sci.* **2025**, *142*, e56686, https://doi.org/10.1002/app.56686.
29. Nguyen, T.T.T.; Pham, T.H.; Bien, T.T.L.; Tran, T.V. Effect of biosynthesized ZnO and Ag/ZnO nanoparticles on bacterial cellulose/polyvinyl alcohol films for strawberry preservation. *Cellulose* **2025**, *32*, 1049-1070, https://doi.org/10.1007/s10570-024-06316-7.
30. Rahmadiawan, D.; Abral, H.; Pratama, M.A.; Kim, H.-J.; Railis, R.M.; Kurniawan, R.; Primandari, S.R.P.; Shi, S.-C.; Mahardika, M. Synergistic effects of Uncaria gambir and zinc oxide in polyvinyl alcohol films for enhanced UV and blue light shielding, antimicrobial properties, and hydrophobicity: improving application performance in sustainable packaging and protective eyewear. *RSC Adv.* **2025**, *15*, 2766-2778, https://doi.org/10.1039/D4RA08801H.
31. Vinayagam, Y.; Venkatraman, G.; Rajeswari, V.D. Sustainable treatment of glass industry wastewater using biogenic Zinc oxide nanoparticles: Antibacterial and photocatalytic efficacy. *Int. Biodeterior. Biodegrad.* **2025**, *200*, 106036, https://doi.org/10.1016/j.ibiod.2025.106036.
32. Badri, A.; El Ghali, S.; Alvarez-Serrano, I.; Hemden, K.; Aloui, F.; Gassoumi, M. Chenopodium exsuccum plant extract for green zinc oxide nanoparticles synthesis: Photocatalytic titan yellow degradation and antioxidant and antibacterial properties. *Inorg. Chem. Commun.* **2025**, *172*, 113724, https://doi.org/10.1016/j.inoche.2024.113724.
33. Albarqouni, Y.; Roney, M.; Chong, K.F.; Thalji, M.R.; Najafi, G.; Abdullah, A. Self-polymerization of dopamine-coated zinc oxide as a potential antibacterial nanoparticle with molecular docking analysis. *Polym. Bull.* **2025**, https://doi.org/10.1007/s00289-025-05874-5.
34. Khajavi, M.Z.; Nikiforov, A.; Morent, R.; Fraeye, I.; Devlieghere, F.; Ragaert, P.; De Geyter, N. Development of plasma-polymerized nanocomposite coatings with targeted antimicrobial activity utilizing glycine-coated ZnO nanoparticles. *Innov. Food Sci. Emerg. Technol.* **2025**, *104*, 104091, https://doi.org/10.1016/j.ifset.2025.104091.
35. Pangprasit, N.; Kongkaew, A.; Saipinta, D.; Pikulkaew, S.; Intanon, M.; Suriyasathaporn, W.; Chaisri, W. Evaluation of antibacterial properties of zinc oxide nanoparticles against bacteria isolated from animal wounds. *Pharmaceutics* **2025**, *17*, 209, https://doi.org/10.3390/pharmaceutics17020209.
36. Elabbasy, M.T.; El Bayomi, R.M.; Abdelkarim, E.A.; Hafez, A.E.-S.E.; Othman, M.S.; Ghoniem, M.E.; Samak, M.A.; Alshammari, M.H.; Almarshadi, F.A.; Elsamahy, T. Antibacterial and Antibiofilm Activity of Green-Synthesized Zinc Oxide Nanoparticles Against Multidrug-Resistant *Escherichia coli* Isolated from Retail Fish. *Molecules* **2025**, *30*, 768, https://doi.org/10.3390/molecules30040768.

37. Vijayakumar, S.; Chen, J.; González-Sánchez, Z.I.; Duran-Lara, E.F.; Divya, M.; Shreema, K.; Hadem, H.; Mathammal, R.; Prasannakumar, M.; Vaseeharan, B. Anti-colon cancer and antibiofilm activities of green synthesized ZnO nanoparticles using natural polysaccharide almond gum (Prunus dulcis). *J. Clust. Sci.* **2023**, *34*, 165-176, https://doi.org/10.1007/s10876-021-02205-2.
38. Senthilkumar, K.; Rajkumar, M.; Vimala, K.; Thangaraj, R.; Kannan, S. Biosynthesis of Gelatin-Coated Zinc Oxide Nanocomposites from Coccinia indica Extract and its Antibacterial, Antioxidant, Anticancer and Wound Healing Properties. *BioNanoScience* **2024**, *14*, 2993-3010, https://doi.org/10.1007/s12668-024-01574-y.
39. Digisu, A.W.; Berhe Yaebyo, A.; Kebede, W.L.; Ahmed, H.M.; Fentie Yemir, T. Photocatalytic Performance of Silver-Doped Zinc Oxide Nanoparticles for Methylene Blue Degradation. *Catal. Lett.* **2025**, *155*, 100, https://doi.org/10.1007/s10562-025-04932-x.
40. Salaheldin, H.; Aboelnga, A.; Elsayed, A. Mycosynthesis of zinc sulfide/zinc oxide nanocomposite using Fusarium oxysporum for catalytic degradation of methylene blue dye, antimicrobial, and anticancer activities. *Sci. Rep.* **2024**, *14*, 32165, https://doi.org/10.1038/s41598-024-81855-4.
41. Gurusamy, M.; Sellavel, M.; Kuppuvelsamy, V. A sustainable green synthesis for photocatalytic and antibacterial activity of zinc oxide nanoparticles using Cucumis maderaspatanus leaf extract. *Desalin. Water Treat.* **2024**, *319*, 100457, https://doi.org/10.1016/j.dwt.2024.100457.
42. Khafaga, D.S.; Eid, M.; Mohamed, M.H.; Abdelmaksoud, M.D.; Afify, M.; El-Khawaga, A.M.; Abdelhakim, H.K. Enhanced anticancer activity of silver doped zinc oxide magnetic nanocarrier loaded with sorafenib for hepatocellular carcinoma treatment. *Sci. Rep.* **2024**, *14*, 15538, https://doi.org/10.1038/s41598-024-65235-6.
43. Kadhum, H.H.; Ibraheem, S.; Jawad, Z.N.; Jeddoa, Z.M.A.; Rasool, K.H.; Jabir, M.S.; Najm, M.A.; Jawad, S.F.; Al-kuraishy, H.M.; Nayef, U.M. Potential pharmaceutical applications and molecular docking study for green fabricated ZnO nanoparticles mediated Raphanus sativus: In vitro and in vivo study. *Nanotechnol. Rev.* **2024**, *13*, 20240113, https://doi.org/10.1515/ntrev-2024-0113.

Publisher's Note & Disclaimer